Journal of Genetic Engineering and Biotechnology 16 (2018) 527–536

HOSTED BY

Contents lists available at ScienceDirect

Journal of Genetic Engineering and Biotechnology

journal homepage: www.elsevier.com/locate/jgeb

Original Article

Synthesis of silver nanoparticles by *Bacillus clausii* and computational profiling of nitrate reductase enzyme involved in production

Koel Mukherjee [a], Rashmi Gupta [b], Gourav Kumar [b], Sarita Kumari [b], Saptaswa Biswas [c], Padmini Padmanabhan [b,*]

[a] *Bioinformatics Laboratory, Bio-Engineering Department, Birla Institute of Technology, Mesra, Ranchi, Jharkhand 835215, India*
[b] *Bioprocess Engineering Laboratory, Bio-Engineering Department, Birla Institute of Technology, Mesra, Ranchi, Jharkhand 835215, India*
[c] *Centre for Energy, Indian Institute of Technology, Guwahati, Assam 781039, India*

ARTICLE INFO

Article history:
Received 6 March 2018
Received in revised form 24 April 2018
Accepted 27 April 2018
Available online 28 June 2018

Keywords:
Biosynthesis
Silver nanoparticles
Nitrate reductase
In-silico characterization
MD simulation

ABSTRACT

Biogenic synthesis of silver nanoparticles using microorganisms has found interest recently since last decade because of their prospect to synthesize nanoparticles of various size, shape and morphology which are eco-friendly. Here, an eco-friendly method for production of silver nanoparticles from ***Bacillus clausii*** cultured from **Enterogermina** is explored. Along with the biosynthesis and conformity test, *in silico* studies was done on NADPH dependent nitrate reductase enzymes from the view point of designing a rational enzymatic strategy for the synthesis. The detailed characterization of the nanoparticles was carried out using UV-Vis spectroscopy, Dynamic Light Scattering (DLS) particle size analysis, Transmission Electron Microscopy (TEM), X-Ray Diffraction (XRD) analysis. Computational profiling and *in silico* characterization of NADH dependent enzymes was carried out based on literature and work done so far. Nitrate reductase sequence was retrieved from NCBI for characterization. Secondary structure was evaluated and verified by JPred as well as SOPMA Tool. Tertiary structure was also modeled by MODELLER and ITASSER parallel and the best structure was selected based on energy values. Structure validation was done by GROMACS and RMSD, RMSF, temperature variation plot were also plotted. Interactions graphs between nitrate reductase and ligand silver nitrate was done through molecular docking using Hex.

1. Introduction

The nanotechnology is the large dynamic research area in recent material science. Nanoparticles reveal novel or enhanced property's base on detailed description such as size, morphology and distribution. There have been remarkable developments in the area of nanotechnology during the recent past years [1], where new methodologies and techniques are generated to produce the nanoparticles with its particular shapes and sizes. Because of their dimension, nanoparticles contain a larger surface area than macro-size material. Nanoparticles with their minute dimension, shows different properties compared towards the bulk shape the similar objects and therefore, supply a lot of novel developments in the area of biosensors, biomedicine, and bio-nanotechnology [2].

Silver is recognized for its antimicrobial properties and have been used for years in the medical area meant for antimicrobial applications and yet have revealed to prevent HIV interaction to host cells [3]. The silver nanoparticles are also reported to be harmless to human and effective against micro-organisms at extremely low amount and lacking any side effects [4]. Silver nanoparticles, because of their huge exact surface area, are extremely active and can play a central function in inhibiting the microorganism development in aqueous and solid media. The antimicrobial action of colloidal silver is influenced through the size of the nanoparticles. Smaller the particle size more is its antimicrobial effect [5]. Now a day, metallic nanoparticles are mainly made from noble metals (i.e., Ag, PT, Au and Pd) [6] and can be used in the field of catalysis, diagnostic biological problems, optoelectronics, and in display devices. Along with the noble metals, silver (Ag) is also preferable in the area of living organisms, biological systems and medicine [7].

Bio-synthesis of silver nanoparticles of dissimilar shapes and sizes is a rising field of research due to their use in a variety of

Peer review under responsibility of National Research Center, Egypt.
* Corresponding author.
E-mail address: padmini@bitmesra.ac.in (P. Padmanabhan).

https://doi.org/10.1016/j.jgeb.2018.04.004
1687-157X/

biological fields. Biological method used for the production of silver nanoparticles, employing microbes [8,9] and plants [10,11] contain high tremendous importance greater than physical and chemical activities due to the use of nontoxic, environment friendly substrates, and moderately easier production procedure at ambient conditions [12]. Furthermore, biomolecules perform as natural stabilizers used for such nanoparticles, thus prevent not just aggregation, but also a more stabilized step than any chemical methods [9]. The production of silver nanoparticles shows an intense color change due to the Plasmon resonance absorption. The surface of a metal has free electrons in the transmission band and positively charged nuclei and they can be excited to specific vibration modes. Therefore, metallic nanoparticles have characteristic optical absorption spectra in the UV-Vis region [13]. The color change during the production is also coupled with the involvement of extracellular enzyme. The enzyme, nitrate reductase which involves in synthesis of silver nanoparticles converts nitrate to nitrite and an electron shuttle is induced thereby reducing the incoming silver ions to silver nanoparticles.

Microbial production of nanoparticles can be done though usual protection of culture and sterilized environment [14]. The first story of bacteria, *Pseudomonas stutzeri* strain producing silver nanoparticles was reported in 1984 [15]. However, significant study of the huge information on bacterial silver Nanoparticles is still missing. Therefore, this mini work summarizes the bacteria mediated production of silver nanoparticles by intracellular enzymes because enzymatic production of silver nanoparticles is fast and non-toxic for human. *In silico* approaches were taken to characterize the nitrate reductase enzyme, a NADPH dependent which has a potential for the production of silver nanoparticles and is not reported till now.

2. Materials and methods

This section describes about the steps of silver nanoparticle production and its size conformation. *In silico* analysis of the nitrate reductase was also carried over to characterize the enzyme which is having key role in the production process.

2.1. Synthesis of silver nanoparticles

Enterogermina 5 ml oral suspension bottle (Manufacturer: Sanofi India Ltd.) was purchased from local medical shop to provide the spores of multi-antibiotic resistant *Bacillus clausii*. The bacterial strain was cultured in nutrient broth (yeast extract, beef extract, peptone, NaCl) and was incubated for 24 h at 37 °C and 150 rpm in shaker incubator. Next day, the sample was centrifuged for 10 min at 10,000 rpm for the removal of all the matter other than cell biomass. Cells were precipitated and further washed by phosphate buffer at the same rpm [9]. The pellet was dissolved in distil water and ultrasonicated for 5 min at 30 s pulse which results in cell lysis for getting intracellular enzyme which was used for production of silver nanoparticles. The ultrasonicated cells were centrifuged for 10 min at 4 °C, 10,000 rpm taking the cell lysate supernatant and discarding the pellet. Two controls (positive control = enzyme & water), (negative control = substrate & water) and one sample (enzyme & substrate) were taken for the synthesis of silver nanoparticles by further making up the volume to 25 ml. All three samples (1 sample and 2 control) were incubated for 24 h at 37 °C in shaker incubator at 150 rpm.

2.2. Conformity test

To confirm the production of silver nanoparticles, samples were first analyzed in a Perkin-Elmer UV-VIS spectrophotometer, Lambda-19. The scanning range for the sample was 400–700 nm. The spectrophotometer was equipped with "UVWinlab" software to record and analyze data. Characterization of silver nanoparticles was done by different method such as Transmission electron microscopy (TEM), dynamic light scattering (DLS), and energy dispersive spectroscopy (EDS) and Zeta size analyzer.

The prepared sample was dispersed in deionized water followed by ultra-sonication after which solution was filtered and centrifuged for 10 min at 25 °C, 5000 rpm. The supernatant was diluted 3–4 times and then the particles in liquid were analyzed for DLS and Zeta potential.

2.3. Retrieval of target and template sequence

The amino acid sequence of nitrate reductase from the species *Bacillus clausii* (GenBank ID: KKI86930.1) was retrieved in FASTA format. Sequence homologies were obtained with HHpred [16] using default setting parameters. Two homologous sequences were selected as templates based on highest score and SS value, query coverage, lowest E-value and P-value, and 90% above identity probability.

2.4. Physiochemical and functional characterization

Using the ProtParam tool of Expasy, molecular weight, theoretical isoelectric point (pI value), total number of negatively (Asp + Glu) and positively (Arg + Lys) charged residues, extinction coefficients [17], instability index [18], aliphatic index [19] and grand average of hydropathicity (GRAVY) [20] were computed. Secondary structural features were predicted with Self Optimized Prediction Method from Alignment (SOPMA) [21]. The domain and motif of the selected protein sequence was screened through NCBI conserved domain and ScanProsite (http://prosite.expasy.org/scanprosite/) server. Disulfide bond prediction is very crucial to understand the function of protein as well as for tertiary prediction methods. DiANNA 1.1 web server (http://clavius.bc.edu/~clotelab/DiANNA/) was used to carry out the study [22].

2.5. Modelling of enzyme

The structure of nitrate reductase was unavailable in Protein Data Bank and thus it was modeled by Modeller (Modeller 9v12) and I-TASSER method [23,24]. Modeller follows the homology modelling algorithm and thus requires template to model the structure. The modeling tool gave a list of 2 suitable templates which were individually aligned with the target protein sequence by local pair wise-alignment method using EMBOSSWATER (http://www.ebi.ac.uk/Tools/psa/emboss_water/) tool of EMBL-EBI (http://www.ebi.ac.uk/). One was nitrate reductase A, from *Escherichia coli* (PDB Id: 1Q16), and another one was perchlorate reductase from *Azospirasuillum* PS (PDB Id: 4YDD). As the former template was having high coverage area, maximum identity, similarity and alignment score with our query so it was selected to generate the 3D model.

The said enzyme structure was modeled again through I-TASSER server which follows the steps of stitching of small fragments of enzymes after part modelling. I-TASSER searches the possible templates in PDB first (with a pair-wise sequence identity cut-off of 70%) and if template is not found then it runs the ab initio method to predict the 3D structure of enzymes. 3D models of enzymes were build based on multiple-threading alignments by LOMETS and iterative TASSER assembly simulations.

2.6. Validation study of 3D model by GROMACS

Ramachandran plot analysis for the modelled enzyme was done using PROCHECK and RAMPAGE [25,26]. Z-score was calculated using interactive ProSA web service for the recognition of errors in three-dimensional structure which indicated model quality and total energy deviation of the structure with respect to energy distribution derived from random conformations.

The best way to verify and validate the modelled structure is to view the trajectories of each and every atoms of the enzyme within a given timeframe of nanosecond scale. The molecular dynamics simulation serves the purpose by mimicking the real condition of a cell inside a box under solvent condition. GROMOS 96-43a1 force fields of GROMACS 4.0 package (DePristo et al., 2005) was applied on the best modeled structure [27]. The 3D structure of the enzyme was taken in a cubic box with a 4.0 Å edge length. The "SPC" water model (spc216.gro file) was used to fill up the box. After the box creation, steps were followed by genion, energy minimization and MD simulation. MD simulation was performed for a period of 10 ns maintaining the temperature at 300 K and pressure at 1 atm [28].

2.7. Interaction study of enzyme

Silver with molecular formula of Ag (ChemSpider Id – 22878) structure information was retrieved from ChemSpider website in mol format and converted to pdb format using Open Babel software. The software Hex 8.0.0 was used for docking study between nitrate reductase and silver nanoparticle. Hex uses geometric hashing or fast Fourier transform (FFT) correlation techniques to find a relatively small number of putative docking orientations which may be refined and re-scored using more sophisticated techniques [29]. Binding sites on model structure for metal ligands was predicted by Site Hound web server. Solvent accessibility analysis was done by ASAView. Accessible surface area (ASA) gives an overview of amino acids present on active sites which in turn also give an overview of dock able regions on the enzyme [30].

Fig. 1. Image of flask showing visible color change, proving the biosynthesis of silver nanoparticles by *Bacillus clausii*.

3. Results & discussions

3.1. Visual observation and analytical results

Silver nanoparticles show evidence of yellowish brown color in aqueous solution due to excitation of surface plasmon resonance. On mixing the intracellular enzyme with an aqueous solution of the silver nitrate, a change in the color from colorless to yellowish brown was observed [31]. The intensity of brown color change is directly proportional to reaction time. It was due to the reduction of Ag+ which indicates the formation of silver nanoparticles shown in Fig. 1.

From literature it was known that silver nanoparticles give its Plasmon resonance peak in between 440–480 nm [32] and as our solution gave the λ max value at 470 nm, thus confirming the presence of silver nanoparticles. It was also observed that the peak in pink color shifted in the absorption spectrum from 350 nm to 480 nm with increasing reaction time (Fig. 2). The work was carried out in the presence of two controls, one having only silver nitrate and other containing bacterial cell lysate. It was prominent from the figure that the third sample which contains both substrate and enzyme gave a peak where as other two failed. So, it can be explained in the way that production of silver nanoparticles requires both the bacterial cell lysate (enzyme) and substrate ($AgNO_3$). The particle size distribution of synthesized silver nanoparticles of the different size histogram shows the silver nanoparticles [33] are in the range of 30–80 with average particle size 58 nm (Fig. 3).

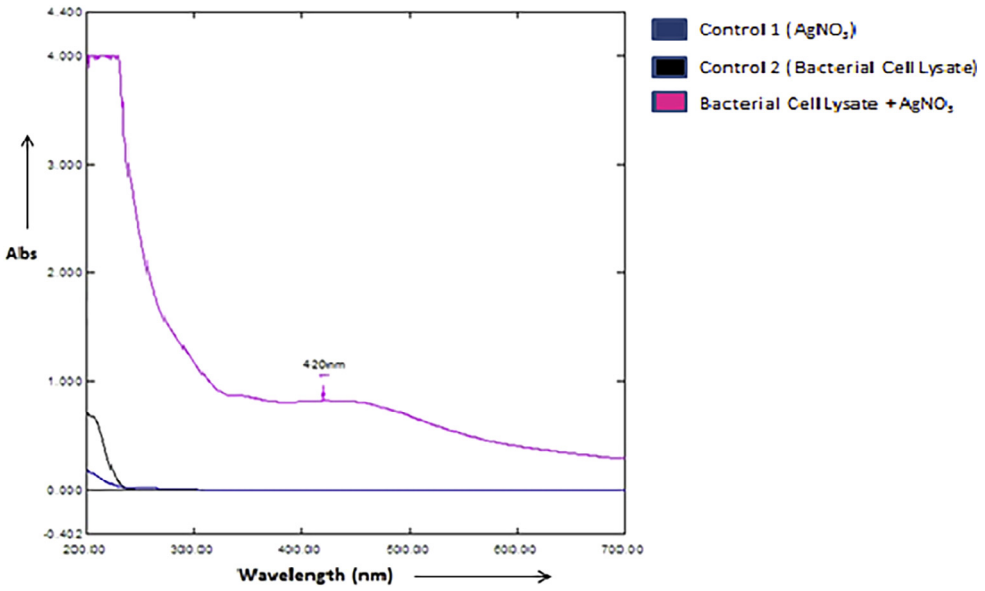

Fig. 2. UV–Vis absorption spectra of synthesized AgNPs by *Bacillus clausii* for 24 h (curve1) for synthesized silver nanoparticles (curve 2 & 3 is for control).

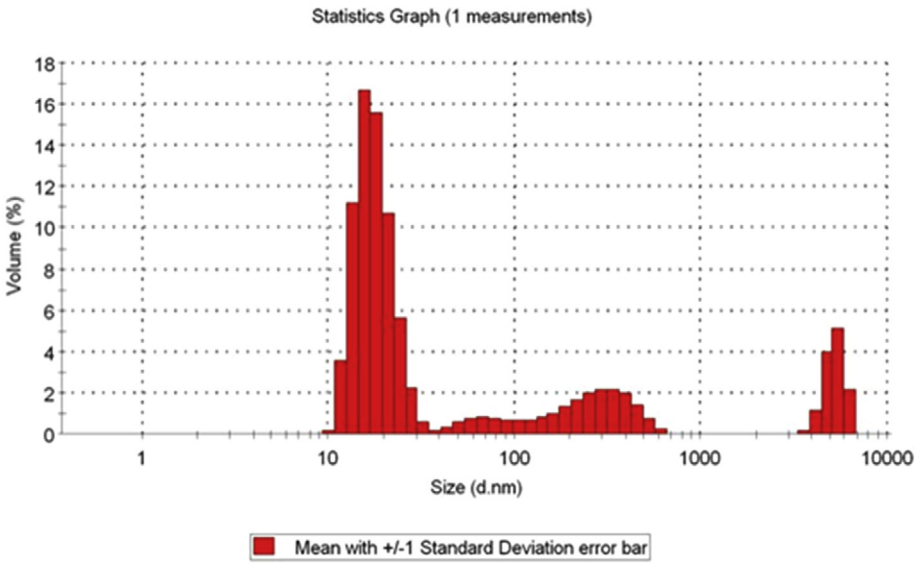

Fig. 3. Particle size distribution histogram (red color) of silver nanoparticles synthesized by *Bacillus clausii*.

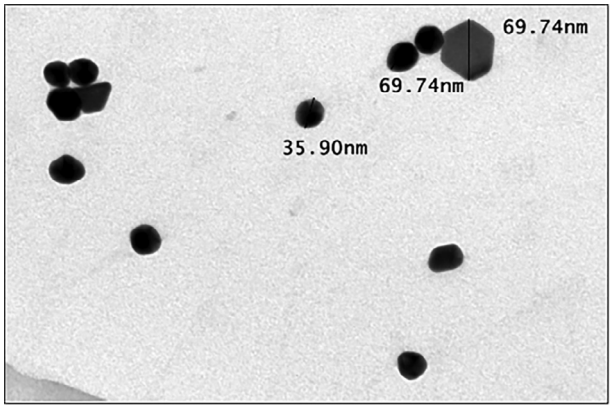

Fig. 4. TEM image of silver nanoparticles by *Bacillus*.

From the plot it was evident that the solution was consist of nanoparticles having various sizes which are indeed in agreement of the result obtained by TEM analysis [34]. The spherical shaped glittering silver nanoparticles can be seen from TEM images and confirmed the development of silver nanostructures (Fig. 4). So, in the process of conformity test of silver nanoparticle production the EDX reading proved that the silver was there in the sample by giving peaks (Fig. 5). The glitter spherical shape silver nanoparticles were confirmed [35].

In the present study silver nanoparticles synthesis was done by ***Bacillus clausii*** with a high probability of some intracellular enzymes. Among the intracellular enzymes, sulfite reductase and nitrate reductase [36] are responsible for electron reduction processes during the synthesis of gold nanoparticles. Both nitrate reductase and sulfite reductase favor multi-electron reduction processes and may share common mechanistic features. Previous work shows the involvement of nitrate reductase in reduction of gold to gold nanoparticles thus further extending the study in that direction only [37]. *In silico* characterization was applied on enzyme, nitrate reductase.

3.2. Sequence and template retrieval

1224 amino acid long sequence of Nitrate reductase in FASTA format (>KKI86930.1 nitrate reductase [*Bacillus clausii*]) (GenBank ID: KKI86930.1) was procured from NCBI. The sequence was then used to find homologous sequences using HHPred (Homology detection & structure prediction by HMM-HMM comparison).

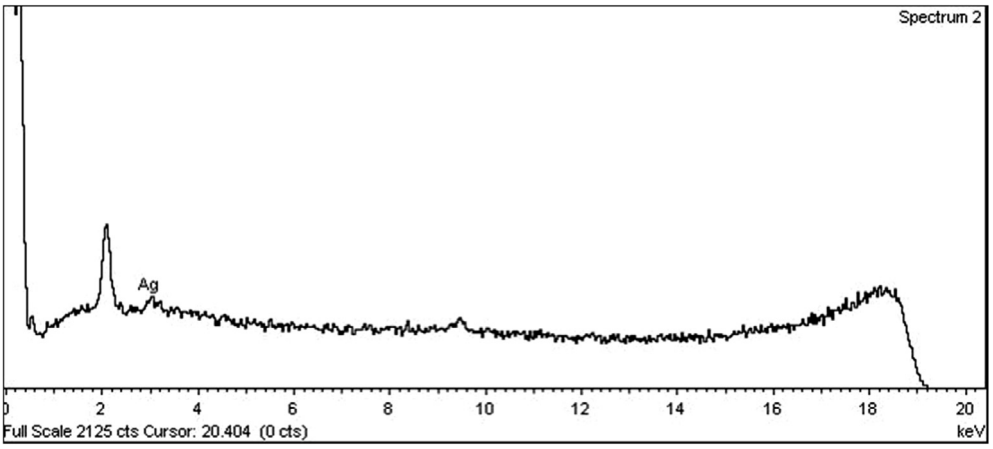

Fig. 5. EDS analysis of silver nanoparticles showing characteristic peaks of silver (Ag).

3.3. Physicochemical analysis and result

Physiochemical properties of the target sequence were computed using ProtParam tool (Table 1). The computed isoelectric point (pI value), extinction coefficient, instability index, aliphatic index and Grand average of hydropathicity (GRAVY) value of the enzyme are shown below. The extinction coefficient calculated gives us a measure of the amount of light absorbed by the protein at a particular wavelength (280 nm). The value for instability index is slightly more than 40 meaning the structure is slightly unstable. Instability index relies upon the occurrence of certain dipeptides along the length of the enzyme. Aliphatic index was computed as 71.57. Higher aliphatic index indicated structural stability. The aliphatic index refers to the relative volume of a protein that is occupied by aliphatic side chains. An increase in the aliphatic index increases the thermo stability of enzyme [36]. Grand average of hydropathicity (GRAVY) value of this enzyme was found to be negative which designates it to be hydrophilic in nature. Secondary structural features of the enzyme using SOPMA are as follows, where significant amount as, 29.82% was helix structure, 20.67% was beta strand and significant amount of random coils are observed.

Table 1
Physiochemical properties of enzyme (nitrate reductase) predicted by ProtParam tool.

S. No.	Parameter	Value
1	Molecular weight	138873.25
2	Theoretical pI	5.72
3	Total number of negatively charged residues (Asp + Glu)	153
4	Total number of positively charged residues (Arg + Lys)	126
5	Extinction coefficients M^{-1} cm^{-1}, at 280 nm	291,660–291,410
6	Instability index	42.05
7	Aliphatic index	71.57
8	GRAVY	- 0.501

The scanning of the sequence was also verified through conserved domain identification and motifs search. The domain and motifs are the area which are conserved for specific functionality and thus can also give some idea about the residues which are shy in nature and thus forming the core part of the protein. The conserved domain analysis predicts NarG Superfamily, stretching from 7th residue to 1221 (Fig. 6A). This nitrate reductase alpha subunit mainly helps in Energy production and conversion, Inorganic ion transport and metabolism. To identify the motif within the said domain, ScanProsite result was also procured [38]. The result shows the region 41–105 residues forming 4Fe-4S oxidoreductase. There are several metal binding sites predicted within the region like residue no. 48, 52, 56 and 91 (Fig. 6B).

Two disulfide bonds are predicted by DiANNA (Table 2). They are essential to study the cross-linkages in proteins which considerably effects protein structure and function [22]. The score is attributed to the distance between the cysteine residues. More distance leads to more score.

3.4. 3D model selection and validation result

The sequence was modelled to give five output sequences. From the five constructed models, one with the lowest Discrete Optimised Protein Energy (DOPE) score was selected. The structure is shown in figure ahead (Fig. 7A). The dope score profile was plotted in Table 3. The best structure was having the lowest DOPE score (**−53758.21**).

The I-TASSER method shows best ten template structure with its PDB hit, normalized Z score of the threading alignment, percentage sequence identity of the whole template (iden1) and in the threading aligned region (iden2), coverage of the threading alignment. Table 4 describes about this information, where it can be noticed that the query sequence is having maximum sequence alignment with two templates, 3IR7A (0.99) and 1Q16A (0.99). I-TASSER method predicted five models of nitrate reductase enzyme structure with different C-score (Confidence score), TM

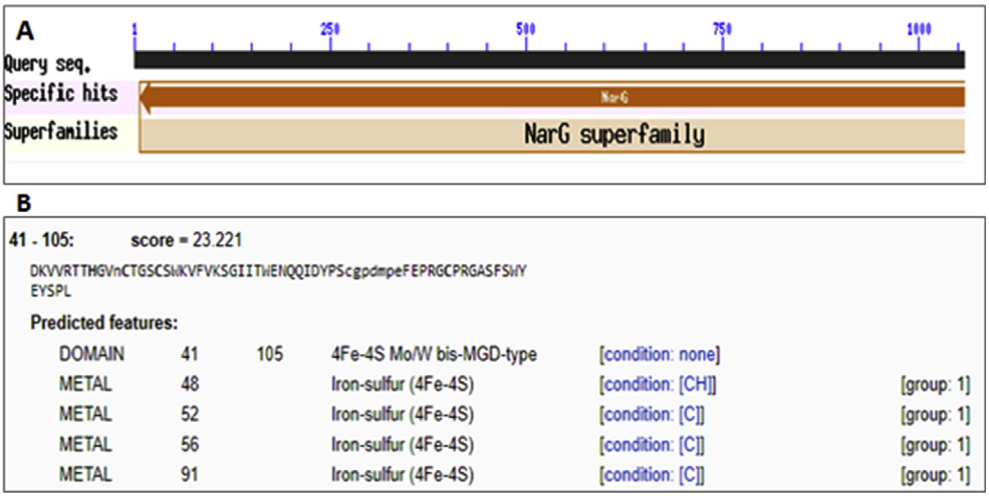

Fig. 6. Sequence analysis of nitrate reductase (A) Domain analysis by Conserved Domain of NCBI (B) active site or motif search by ScanProsite server.

Table 2
Disulfide bonds in Nitrate Reductase.

S. No.	Cysteine sequence position	Bond	Distance	Score
1	52–91	THGVNCTGSCS – FEPRGCPRGAS	39	0.01718
2	79–570	IDYPSCGPDMP – VGQEKCRPIEG	491	0.99978

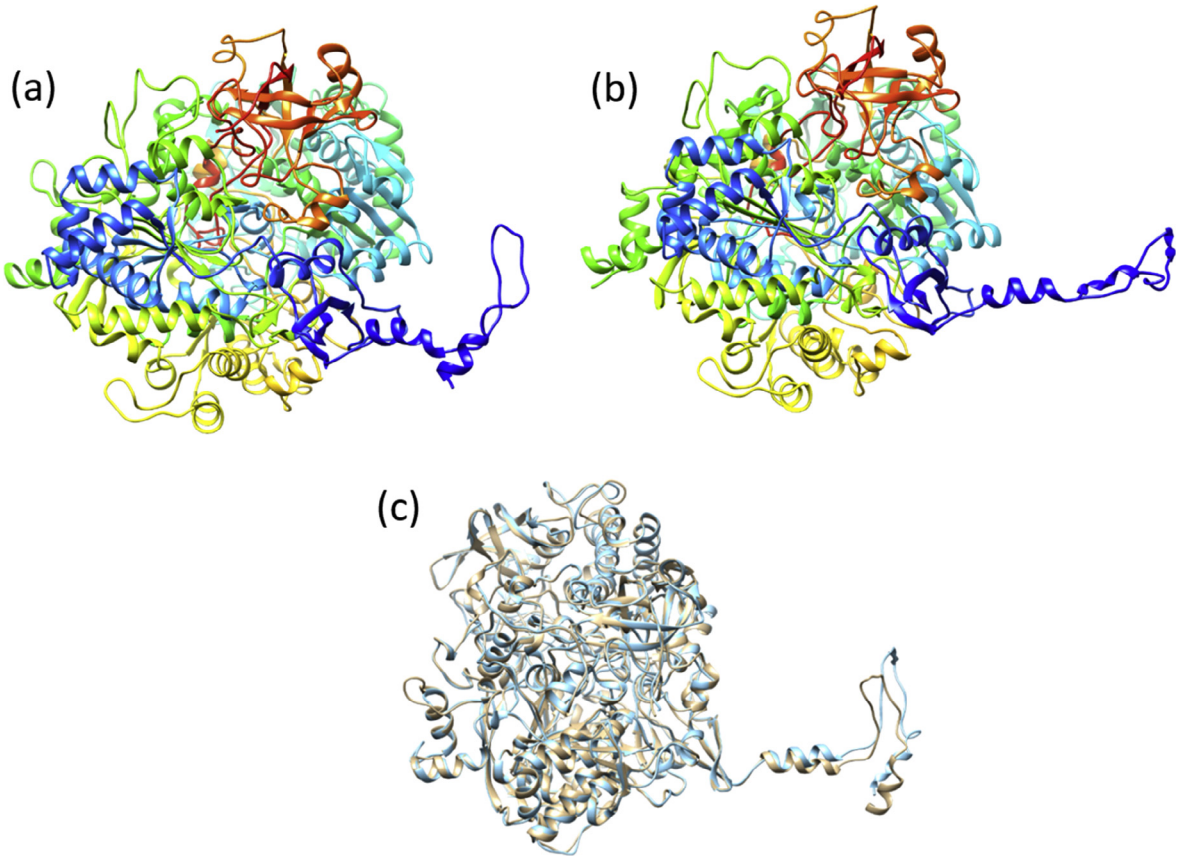

Fig. 7. Screenshot of models generated through Modeller and ITASSER software. (A) Model 1 from modeller result (B) Model 4 from ITASSER result (C) superimposed structure by Chimera.

Table 3
DOPE Score profile of five modeled structure of nitrate reductase through Modeller software.

S. No.	Model name	DOPE score
1	Model 1	−52368.20
2	Model 2	−52467.43
3	Model 3	−53368.97
4	**Model 4**	**−53758.21**
5	Model 5	−52568.34

The best structure was having lowest DOPE score which is highlighted in bold.

score and Root Mean Square Deviation (RMSD) for estimating the quality of predicted structure. The best model (model 1) (Fig. 7B) was selected depending on minimum RMSD value (3.7 ± 2.6 Å) TM score (0.99 ± 0.03) and C-Score (2.0). C-score of higher value signifies a model with a high confidence and vice-versa. To proceed with the best modeled structure both the selected structures from Modeller and ITASSER were superimposed to find the deviation between them. The minimum RMSD was calculated (0.328A) with model 1 and model 4 (Fig. 7C).

The selected models as model 4 from Modeller and model 1 from ITASSER were validated with Ramachandran's plot (Fig. 8A and B) and its statistics value for favored regions and so on. Procheck showed a good percentage value of 88.9% for model 4 and 94.2% for model 1. 9.1% and 3.9% likewise residues are in the allowed region. From the plot statistics it was clear that model 1 was stable more than model 4, so the rest of the work was carried out with this model [40].

Table 4
Top 10 templates used by I-TASSER for structure modelling.

S. No.	PDB Id	Iden1	Iden2	Cov.	Norm. Z Score
1	3IR7A	0.52	0.53	0.99	5.21
2	1Q16A	0.51	0.53	0.99	9.14
3	1Q16A	0.52	0.53	0.99	7.60
4	1Q16A	0.52	0.53	0.99	5.55
5	3IR5A	0.52	0.53	0.98	19.96
6	1Q16A	0.52	0.53	0.99	4.00
7	3IR7A	0.52	0.53	0.99	14.48
8	1Q16A	0.52	0.53	0.99	6.79
9	3EGWA	0.51	0.53	0.97	14.40
10	3IR7A	0.52	0.53	0.99	5.25

*Ident1 is the percentage sequence identity of the templates in the threading aligned region with the query sequence; Ident2 is the percentage sequence identity of the whole template chains with query sequence; Cov. represents the coverage of the threading alignment; Norm. Z-score is the normalized Z-score of the threading alignments.

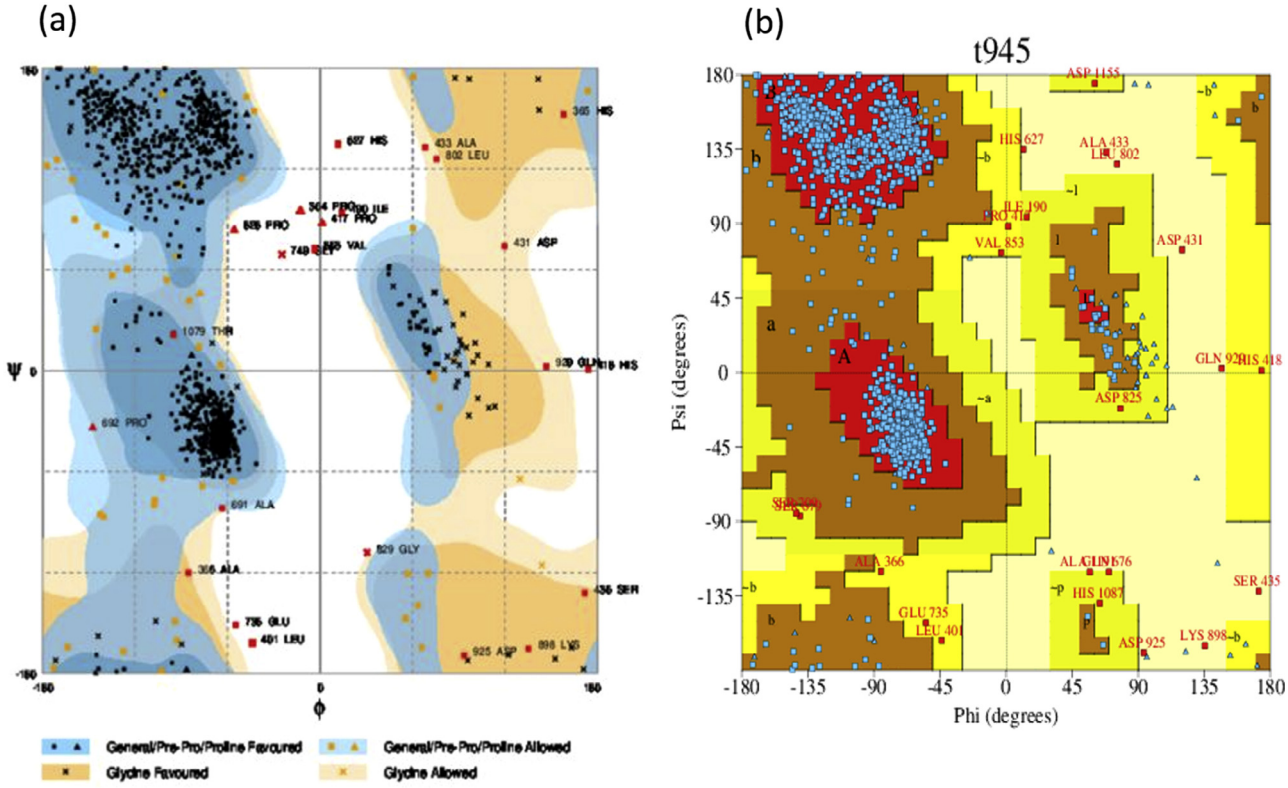

Fig. 8. Ramachandran plot of both the modeled structure (A) Model 4 plot from Rampage (B) Model 1 from Procheck.

The graph generated by ProSA showed overall model quality and location of the Z-score for the structure. It was used to check 3D model of protein for potential errors. The program displayed a plot of its residue energies (Fig. 9). In general, it accepted that positive values correspond to problematic or erroneous parts of a model. Our analysis showed that the predicted structure quality was acceptable as maximum area of the graph is in the negative region.

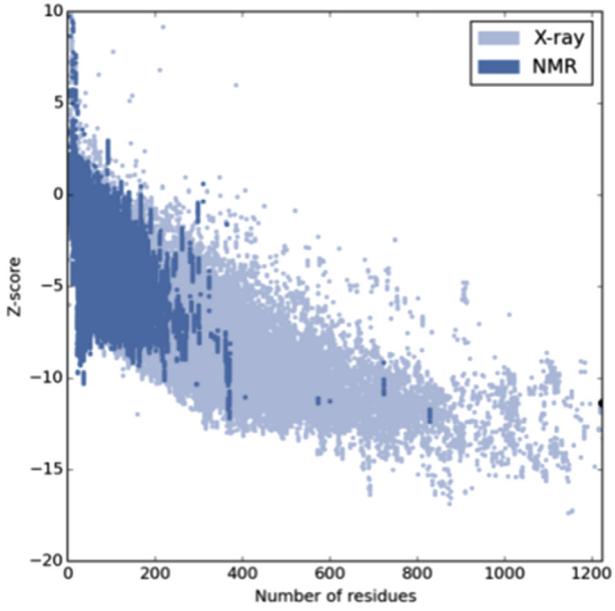

Fig. 9. Z-score analysis using ProSA of Model 1.

3.5. Molecular dynamics study

In order to examine whether the predicted structure of protein remains stable in the presence of explicit solvent from a dynamic point of view, the molecular dynamic simulation was performed. Before simulation, energy minimization was performed by steep and conjugate gradient (cg) methods to regularize the protein structure geometry. After the completion of simulation, the trajectory files were generated, which were analyzed with different tools of GROMACS. GROMACS includes a simple trajectory viewer, ngmx for animation and general visualization but at the same time it also allows user to generate xvg files from the tpr and trr files [39]. The values for each cases of root mean standard deviation (RMSD), radius of gyration (Rg), root mean square fluctuation (rmsf), energy and etc can be individually plotted in excel sheets. Here we plotted the RMSD (Fig. 10) and RMSF curve (Fig. 11) with reference to time scale (10 ns). For both the cases, initial spikes will be there as starting kick of force field [37,38]. RMSD plot shows a less fluctuation after some time and behaves as x-axis parallel. Stability of a modeled structure can be verified from the nature of curve if it is less fluctuating and vibrational [39,40]. Another plot of temperature (Fig. 12) shows the temperature up-down in the simulation process. As the temperature was set at 300 K for the time scale, it can be easily viewed that after 1 ns the average temperature was stable at the said value.

3.6. Docking studies and ASAview result

Key functional properties of proteins and so-called active amino acid sites strongly correlate with amino acid solvent accessibility or accessible surface area (ASA). Probable and promising active sites potentially lie in the higher accessibility region [30]. As can be seen through the table (Table 5) that positively and negatively charged amino acids is highlighted by blue and red circular dots

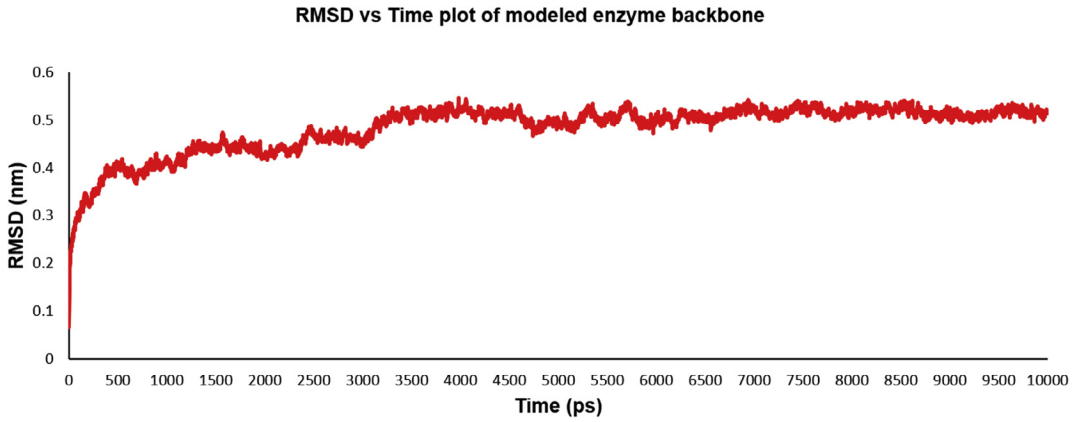

Fig. 10. Backbone RSMD of modeled nitrate reductase (model 1). The red line shows the fluctuation of the backbone with the time scale of 10 ns.

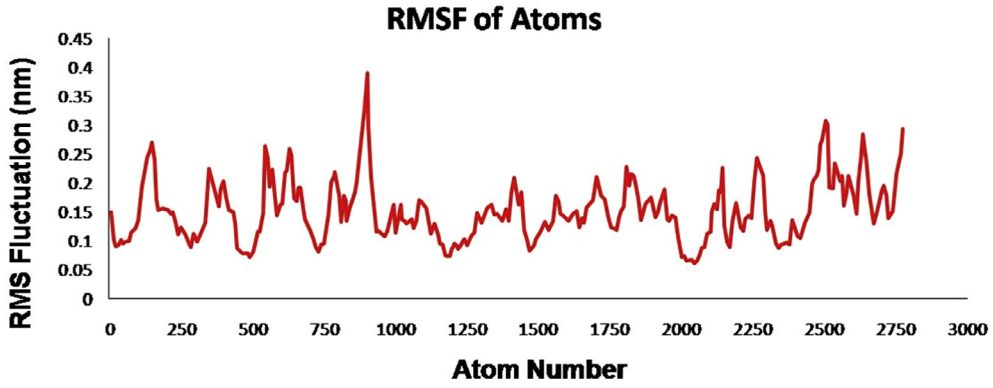

Fig. 11. RMSF of the Cα atom of nitrate reductase. The red line represents the fluctuation of atoms with the time scale of 10 ns.

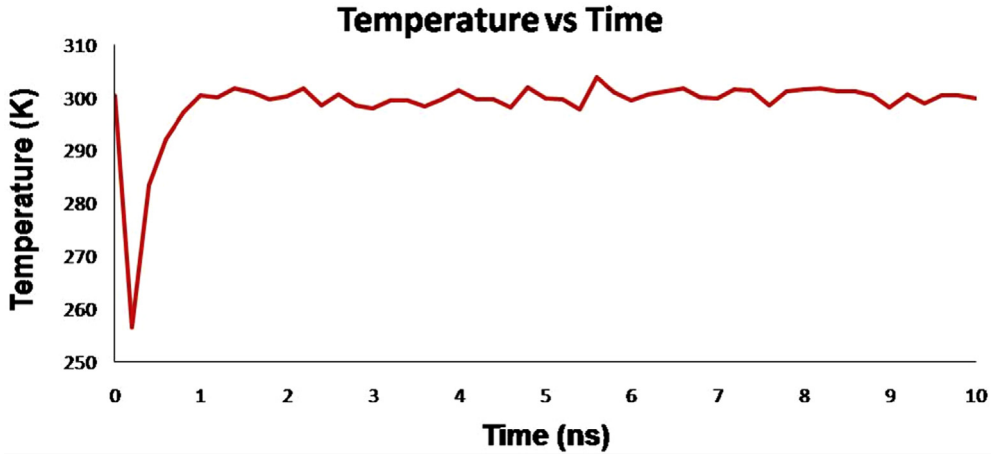

Fig. 12. Temperature variation Stus along the time scale of 10 ns for the system.

Table 5
ASA view result of amino acids.

Color	Category	Amino Acids
Blue	Positive charged residues	R, K, H
Red	Negative charged residues	D, E
Green	Polar uncharged residues	G, N, Y, Q, S, T, W
Yellow	Cystein	C
Grey	Hydrophobic residues	All Others

which are majorly found on the outer ring indicating active amino acids for binding and reactions of the protein (Fig. 13).

The modeled structure of nitrate reductase was used as the receptor molecule and silver was used as the ligand. Docking was performed using default parameters. Cysteine and Histidine metal binding sites and ligand binding sites were predicted using Site Hound web server (Table 6). The ligand binding sites were identified by computing the interactions between the chemical probe Methyl Carbon (CMET) and the target enzyme sequence. 10 regions

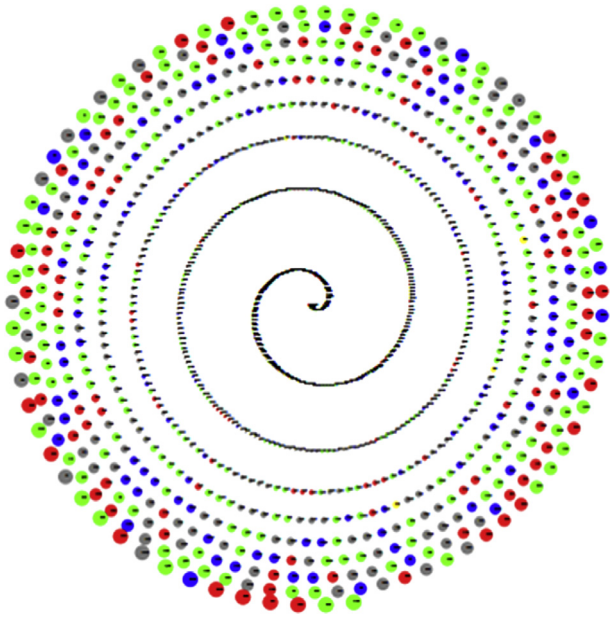

Fig. 13. Graphical representation of solvent accessibility of amino acids in nitrate reductase.

with different levels of energy had been recognized by the web server. The highest energy is related to ligand bound to enzyme at a position which is equal to −1570.77.

The docking was successful and Fig. 14 shows a zoomed – in view of the enzyme showing the interaction between the ligand – silver nitrate and the receptor - nitrate reductase. The location of the ligand binding site in the enzyme as given by docking is consistent with the I-TASSER results. The binding of silver nitrate with the enzyme proves that the enzyme nitrate reductase from *Bacillus clausii* is able to produce silver nanoparticle and can be efficiently used in drug delivery systems

In order to scale up the process of nanoparticle production, we can specifically target the protein nitrate reductase responsible for silver nanoparticle biosynthesis through *Bacillus clausii*. Detailed analysis and computational profiling of the reductase enzyme was performed to highlight the physicochemical characteristics and structural orientation. Better understanding of the enzymes on the proteomics level will help us to devise more efficient downstream processing strategies and practices. Further, with the information and data of this research, the authors intend to proceed forward the work by immobilizing the enzyme nitrate reductase. As, immobilization leads to absence of enzyme with the products, so purification or downstream processing charges are heavily reduced. At the same time these immobilized enzymes will be available for immediate use which ensures continuity of silver nanoparticle production.

4. Conclusion

Chemical and physical methods are becoming more harmful methods for the nanoparticle production nowadays. A green synthesis or using microbes is more economic and easily finished approach. Here in this work we tried to synthesis silver nanoparticles from *Bacillus clausii* as there were no studies before our work. Wither nanoparticles have been produced or not, was verified by many conformity test. The average size of nanoparticles was

Table 6
Ligand binding sites by Site Hound web server.

Rank	Energy	Energy range	Volume	Center (x,y,z)
1	−1570.77	(−18.31, −8.99)	130.00	−129.900 −81.896 −28.145
2	−1461.04	(−19.08, −8.90)	104.00	−126.987 −61.167 −27.478
3	−1295.21	(−16.08, −8.91)	116.00	−111.230 −81.736 −0.161
4	−1220.34	(−18.26, −8.93)	95.00	−130.467 −67.860 −7.236
5	−1193.80	(−20.29, −8.92)	97.00	−103.105 −89.336 −17.815
6	−1119.67	(−18.52, −8.96)	97.00	−99.405 −62.821 −33.958
7	−924.10	(−16.84, −8.97)	82.00	−109.792 −98.039 −10.976
8	−871.73	(−17.84, −8.90)	80.00	−116.405 −46.509 −21.269
9	−807.42	(−18.75, −8.98)	68.00	−126.288 −84.947 −42.937
10	−708.91	(−20.92, −9.00)	47.00	−133.218 −64.749 −17.214

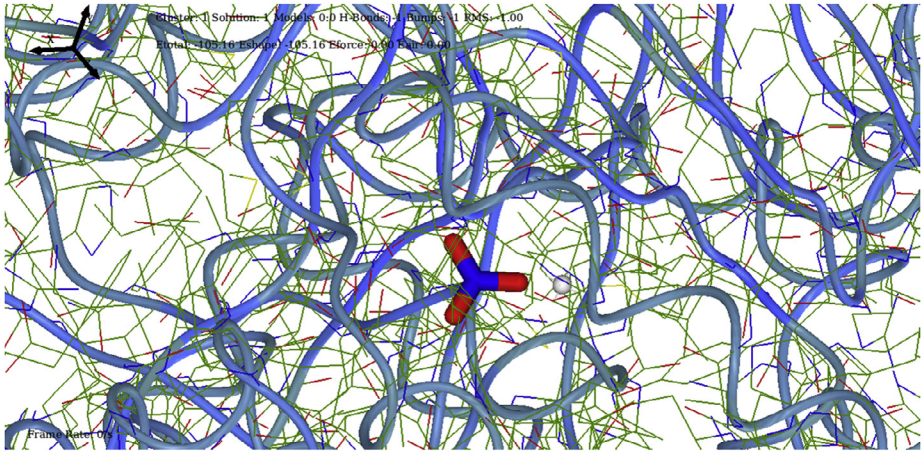

Fig. 14. Hex Dock view of interaction between silver nitrate and nitrate reductase.

around 150 nm scale. It was known from literature survey that the enzyme Nitrate reductase converts silver nitrate to silver nanoparticles. Also, through literature survey a list of microorganisms involved in silver nanoparticles was made and it was found that maximum of these organisms contained nitrate reductase. With green synthesis of nanoparticles, *in silico* approaches were also taken to profile the enzyme nitrate reductase. With better understand of structure and behavior of enzyme, we look forward to establishing an enzyme immobilized system with pure nitrate reductase that can be reused multiple times which may lead to higher productivity of silver nanoparticle at lower cost. This would help the authors to produce silver nanoparticles on commercial level making it a cost effective industrial process.

Acknowledgements

The authors acknowledge BTISnet, Department of Biotechnology, Government of India and TEQIP-II, Birla Institute of Technology for providing Infrastructure facility for Bioinformatics.

References

[1] Chinnadayyala SR, Santosh M, Singh NK, Goswami P. Alcohol oxidase protein mediated *in- situ* synthesized and stabilized gold nano particles for developing amperometric alcohol biosensor. Biosens Bioelectron 2015;69:155–61.
[2] Albrecht AM, Evans CW, Raston CL. Green chemistry and the health implications of nanoparticles. Green Chem 2006;8:417–32.
[3] Baker C, Pradhan A. Synthesis and antibacterial properties of silver nanoparticles. J. Nanosci Nanotechnol 2005;5(2):244–9.
[4] Singh R, Shedbalkar UU, Wadhwani SA, Chopade B. Bacteriagenic silver nano particles: synthesis mechanism and application. Appl Microbiol Biotechnol 2015;99(11):4579–93.
[5] Verma VC, Kharwar RN, Gange AC. Biosynthesis of antimicrobial silver nanoparticles by the endophytic fungus *Aspergillus clavatus*. Nanomedicine 2010;5:33–40.
[6] Sastry M, Ahmad A, Islam NI, Kumar R. Biosynthesis of metal nanoparticles using fungi and actinomycete. Current Sci 2003;85:162–70.
[7] Parashar V, Parashara R, Sharmab B, Pandey AC. Parthenium leaf extract mediated synthesis of silver nanoparticles: a novel approach towards weed utilization. Dig J Nanomater Biostruct 2009;4(1):45–50.
[8] Ahmad A, Mukherjee P, Senapati S, Mandal D, Khan MI, Kumar R, et al. Extracellular biosynthesis of silver nanoparticles using the fungus *Fusarium oxysporum*. Colloids Surf B 2003;28:313–8.
[9] Li S, Shen Y, Xia A, Qiu L, Zhang L. Green synthesis of silver nanoparticles using *Capsicum annuum* L. extract. Green Chem 2007;9:852–8.
[10] Jain D, Daima HK, Kuchhwaha S, Kothari SL. Plant mediated silver nanoparticles using papaya fruit extract and evaluation of their antimicrobial activities. Dig J Nanomater Biostruct 2009;4(3):557–63.
[11] Ghosh S, Patil S, Ahire M, Kitture R, Kale S, Pardesi K, et al. Synthesis of silver nanoparticles using Dioscorea bulbifera tuber extract and evaluation of its synergistic potential in combination with antimicrobial agents. Int J Nanomed 2012;7:483–96.
[12] Wang ZL. Nano-piezotronics. Adv Mater 2007;19(6):889–92.
[13] Kulkarni N, Muddapur U. Biosynthesis of metal nanoparticles: a review. J Nanotechnol 2014:1–8.
[14] Klaus T, Joerger R, Olsson E, Granqvist CG. Silver-based crystalline nanoparticles, microbially fabricated. Proc Natl Acad Sci 1999;96:13611–4.
[15] Altschul SF, Gish W, Miller W, Myers EW, Lipman DJ. Basic local alignment search tool. J Mol Bio 1990;215(3):403–10.
[16] Guruprasad K, Reddy BB, Pandit MW. Correlation between stability of a protein and its dipeptide composition: a novel approach for predicting in vivo stability of a protein from its primary sequence. Protein Eng Des Sel 1990;4(2):155–61.
[17] Ikai A. Thermostability and aliphatic index of globular proteins. J Biochem 1980;88(6):1895–8.
[18] Kyte J, Doolittle RF. A simple method for displaying the hydropathic character of a protein. J Mol Bio 1982;157(1):105–32.
[19] Geourjon C, Deleage G. SOPMA: significant improvements in protein secondary structure prediction by consensus prediction from multiple alignments. Bioinformatics 1995;11(6):681–4.
[20] Ferrè F, Clote P DiANNA 1.1: an extension of the DiANNA web server for ternary cysteine classification. Nucl Acids Res 2006;34(suppl_2):W182–5.
[21] Kherraz K, Kherraz K, Kameli A. Homology modeling of ferredoxin-nitrite reductase from Arabidopsis thaliana. Bioinformation 2011;6(3):115.
[22] Bonato P, Alves LR, Osaki JH, Rigo LU, Pedrosa FO, Souza EM, et al. The NtrY–NtrX two-component system is involved in controlling nitrate assimilation in Herbaspirillum seropedicae strain SmR1. FEBS J 2016;283(21):3919–30.
[23] Sisinni L, Cendron L, Favaro G, Zanotti G. Helicobacter pylori acidic stress response factor HP1286 is a YceI homolog with new binding specificity. FEBS J 2010;277(8):1896–905.
[24] Masuda T, Suzuki M, Inoue S, Song C, Nakane T, Nango E, et al. Atomic resolution structure of serine protease proteinase K at ambient temperature. Sci Rep 2017;2017:7.
[25] DePristo MA, de Bakker PI, Johnson RJ, Blundell TL. Crystallographic refinement by knowledge-based exploration of complex energy landscapes. Structure 2000;13(9):1311–9.
[26] Dumitraşcu L, Stănciuc N, Aprodu I. New insights into xanthine oxidase behavior upon heating using spectroscopy and in silico approach. Int J Bio Macromol 2016;88:306–12.
[27] Macindoe G, Mavridis L, Venkatraman V, Devignes MD, Ritchie DW. HexServer: an FFT-based protein docking server powered by graphics processors. Nucl Acids Res 2010; 38(suppl_2):W445–9.
[28] Ahmad S, Gromiha M, Fawareh H, Sarai A. ASAView: database and tool for solvent accessibility representation in proteins. BMC Bioinf. 2004;5(1):51.
[29] Kumar SA, Abyaneh MK, Gosavi SW, Kulkarni SK, Pasricha R, Ahmad A, et al. Nitrate reductase-mediated synthesis of silver nanoparticles from $AgNO_3$. Biotechnol Lett 2007;29(3):439–45.
[30] Abdullah NI, Ahmad MB, Shameli K. Biosynthesis of silver nanoparticles using Artocarpus elasticus stem bark extract. Chem Cent J 2015;9(1):61.
[31] Mamatha R, Khan S, Salunkhe P, Satpute S, Kendurkar S, Prabhune A. Rapid synthesis of highly monodispersed silver nanoparticles from the leaves of Salvadora persica. Mater Lett 2017;205:226–9.
[32] Skandalis N, Dimopoulou A, Georgopoulou A, Gallios N, Papadopoulos D, Tsipas D, et al. The effect of silver nanoparticles size, produced using plant extract from arbutus unedo, on their antibacterial efficacy. Nanomater 2017;7(7):178.
[33] Mohanta YK, Panda SK, Bastia AK, Mohanta TK. Biosynthesis of silver nanoparticles from Protium serratum and investigation of their potential impacts on food safety and control. Front Microbiol 2017;8.
[34] Gupta R, Mukherjee K, Singh S. *In silico* characterization of nitrate reductase involved in gold nano particles synthesis in *Pseudomonas denitrificans*. J Pharm Bio Sci 2014;5(3):376–88.
[35] Iravani S, Korbekandi H, Mirmohammadi SV, Zolfaghari B. Synthesis of silver nanoparticles: chemical, physical and biological methods. Res Pharm Sci 2014;9(6):385–406.
[36] Beller HR, Han R, Karaoz U, Lim H, Brodie EL. Genomic and physiological characterization of the chromate-reducing, aquifer-derived firmicute Pelosinus sp. strain HCF1. Appl Environ Microbiol 2013;79(1):63–73.
[37] Lindahl E, Hess B, Van Der Spoel D. GROMACS 3.0: a package for molecular simulation and trajectory analysis. J Mol Model 2001;7(8):306–17.
[38] Rungta D, Chauhan N, Mukherjee K. Identification of Hiv1 protease inhibitor through molecular modelling and structure based virtual screening approach. JABAR 2014;5(3):140–9.
[39] Roy D, Mukherjee K. Homology modeling and docking studies of human chitotrisidase with its natural inhibitors. J Prot Proteom 2015;6(2):183–96.
[40] Pramanik K, Ghosh PK, Ray S, Sarkar A, Mitra S, Maiti TK. An in silico structural, functional and phylogenetic analysis with three dimensional protein modeling of alkaline phosphatase enzyme of *Pseudomonas aeruginosa*. Genet Eng Biotechnol J 2017;15(2):527–37.